Quantum Adsorbates: Path Integral Monte Carlo Simulations of Helium in Silicalite

Charusita Chakravarty

Department of Chemistry, Indian Institute of Technology-Delhi, Hauz Khas, New Delhi 110016, India

Received: July 17, 1996; In Final Form: November 6, 1996[⊗]

Quantum effects on ^{3}He and ^{4}He sorption in silicalite were studied using Fourier path integral Monte Carlo simulations. A helium−silicalite interaction potential was constructed on the basis of the Kiselov model. Simulations were performed over a temperature range 7.5−50 K in the dilute limit when interparticle interactions are negligible. Quantum delocalization was shown to reduce isosteric heats of sorption by up to 25% and specific heats by up to 60% in this temperature range. The difference between the isosteric heats of sorption of ^{3}He and ^{4}He was found to be less that 3% at the temperatures studied. The quantum and classical potential energy distributions were monitored as a function of temperature and were shown to be substantially different below 20 K. The strong potential exerted by the zeolite lattice was shown to appreciably reduce the extent of quantum fluctuations.

1. Introduction

Zeolites are complex, microporous aluminosilicate structure with aluminum−oxygen and silicon−oxygen tetrahedra forming the basic building blocks. The wide diversity in structure, size, and dimensionality of channel networks exhibited by the zeolites allows them to act as molecular sieves as well as to display a range of catalytic behavior.[1,2] In the past decade, molecular dynamics and Monte Carlo simulations have been widely used to study sorption in zeolites.[3−7]

Rare gases form the simplest category of sorbates since they are unreactive and are characterized only by their van der Waals radii and polarizability. A study of rare gas sorption in zeolites is useful for establishing the role of molecular size and polarizability in the thermodynamic and transport properties of sorbates in microporous solids.[1,2] The recent popularity of ^{129}Xe NMR as a technique for probing surfaces and microporous materials has added to the interest in the sorption properties of rare gases.[8−10] The lightest rare gas He is similar in size and mass to molecular hydrogen, H_2; given the catalytic importance of H_2 adsorption, this fact in itself is sufficient to provoke interest in the sorption behavior of helium in zeolites. An additional reason for interest in helium adsorption is the potential use of ^{3} He NMR as a probe of adsorbate structure.[11] One can reasonably expect that ^{3}He and ^{129}Xe NMR spectra will give complementary information on adsorbate structure given the large size and polarizability differences.

Bulk liquid helium is a quantum fluid at low temperatures, which undergoes a superfluid transition at 2.172 K. The effect of confining media on the superfluid transition characteristics is of considerable conceptual interest and has consequently attracted much experimental and theoretical work; confining media studied range from graphite surfaces, Vycor (random silica glass with 30% porosity), aerogel (random silica glass with 98% porosity), zeolites, and fullerites.[12−17] The zeolitic frameworks in which He adsorption has been studied experimentally include silicalite (ZSM-5), ZSM-23, Na-Y, silica-Y, and K-L zeolite.[18−22] Heat capacities and isosteric heats of sorption provide no signatures of the superfluid transition for temperatures as low as 0.1 K, but interesting differences between ^{3}He and ^{4}He sorption isotherms are found. Neutron diffraction studies have recently been employed to study helium and neon adsorption in zeolites.[23]

Several theoretical and computational approaches have been evolved to understand the complex many-body quantum effects involved in low-temperature He adsorption. The quantum density functional approach has been used extensively to map phase diagrams of He in contact with a variety of adsorbents.[15,16] Finite temperature path integral Monte Carlo (PIMC) methods have been used with great success to understand the superfluid transition in bulk ^{3}He and to model helium adsorption on graphite.[17,24,25] Recently Mahanti et al. have modeled ^{3}He (^{4}He) atoms located in adsorption sites using Mott−Hubbard (Bose−Hubbard) models.[26,27] To date no finite temperature quantum Monte Carlo simulations of helium in zeolites have been reported though they would appear to be essential for connecting experiments with simple theoretical models.

In the present work, we have developed the basic framework for finite temperature path integral simulations of helium in zeolites. The primary objective of the present study was to quantify the extent of quantum effects on ^{3}He and ^{4}He sorption in zeolites as a function of temperature. Orthorhombic silicalite was chosen as the sorbent since some experimental work has been initiated on this system.[18] A physically reasonable potential energy function for the helium−silicalite interaction is described in section 2. The Fourier path integral Monte Carlo methodology for studying helium adsorption in zeolites is described in section 3. Simulations of helium in silicalite were focused on the dilute limit when sorbate−sorbate interactions were negligible. Since the temperatures are low, a rigid zeolite lattice was assumed. The computational details and results are presented in sections 4 and 5, respectively. Conclusions are presented in section 6.

2. Potential Energy Surface

The potential energy surface for the rare gas zeolite interaction was based on the Kiselov model.[28−30] The Kiselov model assumes that the Si/Al atoms of the lattice are effectively shielded from interaction with the sorbate by the oxygen tetrahedra. Zero charge is ascribed to the Si and Al atoms. The positive charges on the framework cations are compensated by assigning partial charges to the framework oxygen atoms. The interaction between the zeolite framework and a simple sorbate such as a rare gas atom is then assumed to consist of two components: a dispersion term and an electrostatic induction term. The Kiselov model has been extensively used in

[⊗] Abstract published in *Advance ACS Abstracts,* February 1, 1997.

S1089-5647(96)02155-4 CCC: $14.00

TABLE 1: Potential Energy Parameters for the Kiselov Representation for a Rare Gas in Silicalite

R	ϵ_{RO} (kJ mol^{-1})	σ_{RO} (Å)	ϵ_{RR} (kJ mol^{-1})	σ_{RR} (Å)
He (set A)	0.426	2.49	0.085	2.28
He (set B)	0.426	2.62	0.085	2.28
Ne	0.529	2.78	0.280	2.85
Ar	1.085	3.03	1.184	3.35

simulations of sorbate−zeolite systems and, despite its simplicity, found to provide reasonable results in comparison with experiment.[3−7] A recent attempt has been made to improve the Kiselov model for argon−silicalite by including an additional three-body dispersion term as well by improving the representation of the repulsive interactions;[31] this results in a somewhat narrower channel size and a softer zeolite wall, but the contribution of the three-body term and induction terms is found to be negligible. Thus, the Kiselov model can be considered an adequate starting point for developing a reliable helium−zeolite interaction potential.

Since silicalite is the pure siliceous form of ZSM-5, there are no framework cations, and therefore preservation of electroneutrality does not require assigning of partial charges on lattice oxygens. This removes the contribution of the induction term to the potential energy. The dispersion contribution is written as

$$V_D = 4\epsilon_{OR}\sum_j \left(\frac{\sigma_{OR}^{12}}{r_{ij}^{12}} - \frac{\sigma_{OR}^{6}}{r_{ij}^{6}}\right) \quad (1)$$

where j represents summation over all framework atoms, r_{ij} is the distance between a sorbate atom i and a framework atom j, and ϵ_{OR} and σ_{OR} are the Lennard-Jones well depth and size parameters, respectively, for the rare gas−oxygen dispersion interaction. The van der Waals minimum, r_{OR}, for the oxygen−rare gas bond is assumed to be the sum of the van der Waals radii for the two atoms; then $\sigma_{OR} = 2^{-1/6}r_{OR}$. The well depth, ϵ_{OR}, of the Lennard-Jones potential is given in cgs units by

$$\epsilon_{OR} = \frac{3e^2a_0^{1/2}\alpha_O\alpha_R}{8\sigma_{OR}^6(\sqrt{\alpha_O/n_O} + \sqrt{\alpha_R/n_R})} \quad (2)$$

where α_i is the static polarizability of atom i, i = O or R, and n_i is the number of electrons of atom i.

The Lennard-Jones parameters for the rare gas−silicalite interaction are available in the literature for all rare gases other than helium.[30] The helium−silicalite potential was therefore derived on an analogous basis. The helium−helium interactions were characterized by Lennard-Jones parameters $\epsilon_{RR} = 10.22$ K and $\sigma_{RR} = 2.556$ Å.[32] The polarizability and van der Waals radii of all framework oxygens were taken from ref 30. The static polarizability of He was taken as 0.2050 Å^3.[33] This set of potential parameters is labeled as set A in Table 1. However, with these parameters the helium−silicalite potential has two very confined isolated potential energy wells centered at approximately (4,1.3,1.0) and (4,1.3,5) within the asymmetric unit. These "potential wells" are a spurious feature due to the small size of the helium atom and the assumption made in the Kiselov potential that the silicon atoms are completely shielded from direct interaction with the sorbate by the oxygen tetrahedra. To overcome this problem the σ_{OR} value was increased by ∼7%. This new set of parameters (set B) was used in all the simulations reported here. This small change in parameters was sufficient to limit the size of the potential holes significantly and ensure that these regions are not accessed during MC simulations. Table 1 gives the two sets of potential parameters for helium, as well as those for neon and argon taken from ref 30. In general, for any given site the binding energy of the He−silicalite potential is about half that of the Ne−silicalite potential and about one-sixth that of the Ar−silicalite potentials.

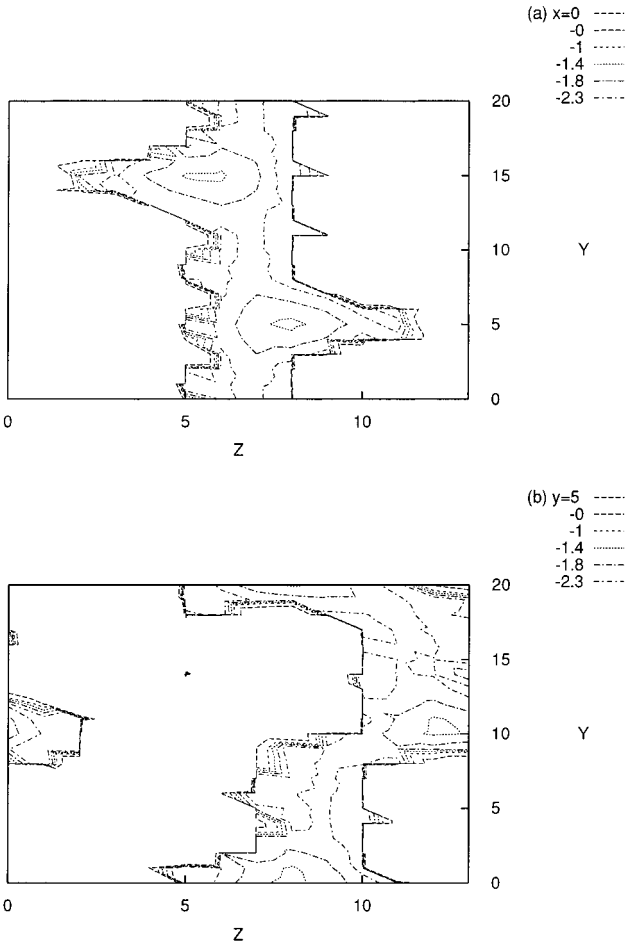

Figure 1. Contour plots of the helium−silicalite potential energy surface using potential parameters in set B: (a) $x = 0$ Å, (b) $y = 5$ Å planes. All distances are in angstroms.

To understand the external potential imposed by the silicalite lattice on an iterant helium atom, it is necessary to consider the silicalite framework structure. Silicalite can exhibit a transition at 340 K from monoclinic to orthorhombic structure.[34] Since the experiments were analyzed on the basis of the orthorhombic structure,[18] we have restricted our simulations to the orthorhombic framework as well. The space group of orthorhombic silicalite is *Pnma*, and the unit cell parameters are $a = 20.07$ Å, $b = 19.92$ Å, and $c = 13.42$ Å.[34] The asymmetric unit is defined as $0 \le x \le 0.5a$, $0 \le y \le 0.25b$, $0 \le z \le c$. The orthorhombic silicalite structure contains two sets of interconnected channels: a series of straight channels parallel to the (010)-direction and a series of zigzag or sinusoidal channels in the (110)-direction. Figure 1a shows a cut through the silicalite lattice at $x = 0$ Å, which effectively bisects the straight channel. The intersections with the sinusoidal channel can be seen in the characteristic widening of the pore size in the z-direction. A cut through the unit cell at $y = 5$ Å effectively bisects a sinusoidal channel running parallel to the (100)-direction, which is shown in Figure 1b.

3. Path Integral Monte Carlo: Observables and Techniques

In the present study, we use the Fourier path integral Monte Carlo technique (FPIMC) to study helium adsorption in a zeolite

lattice at finite temperatures. The FPIMC technique was originally developed by Freeman and Doll[35,36] and has been extensively used for simulations of Lennard-Jones clusters.[37,38] The formalism is presented for a system of interacting distinguishable particles (helium atoms) in an external potential imposed by the framework atoms of the zeolite. In case particle exchange is important, as in bulk helium or helium adsorbed in Vycor, path integral techniques can be suitably adapted.[24,25]

The canonical partition function, Q, can be written as a path integral in imaginary time of the form

$$Q = \int_0^{\beta\hbar} D(\mathbf{x}(u)) \exp\{-S(\mathbf{x}(u))\} \tag{3}$$

where u is the imaginary time coordinate, β is the inverse temperature, $\mathbf{x}$ is the vector corresponding to the Cartesian coordinates of all N particles of the system, $\int_0^{\beta\hbar} D(\mathbf{x}(u))$ represents the set of all cyclic trajectories starting at $\boldsymbol{x}$ at time $u = 0$ and ending at $\boldsymbol{x}$ at time $u = \beta\hbar$, and $S(\mathbf{x}(u))$ corresponds to the Euclidean action evaluated along a given trajectory. The Euclidean action is the sum of kinetic and potential energy terms

$$S(\mathbf{x}(u)) = \frac{1}{\hbar}\int_0^{\beta\hbar} \mathrm{d}u \left[\sum_{i=1}^{N} \frac{m}{2}\left[\frac{\mathrm{d}x_i}{\mathrm{d}u}\right]^2 + V(\mathbf{x}(u))\right] \tag{4}$$

where m is the mass of a single particle and $V(\mathbf{x}(u))$ is the potential as a function of path.

In the FPIMC approach, each quantum path, $\mathbf{x}(u)$, is described in terms of displacements about the classical path, $\mathbf{x}_c(u)$ as

$$x_i(u) = x_{i,c} + \sum_{k=1}^{\infty} a_{k,i} \sin\left(\frac{k\pi u}{\beta\hbar}\right) \tag{5}$$

where x_i denotes a Cartesian component of the ith particle, and the vector $\mathbf{a}_k$ corresponds to the set of kth Fourier coefficients of all the N particles in the system. The kinetic energy term in the action S can then be written very simply as $\sum_k(\mathbf{a}_k^2/2\sigma_k^2)$, where $\sigma_k^2 = 2\beta\hbar^2/m(k\pi)^2$ and the sum over k is truncated at some value k_{max}. In this work a partial averaging procedure is employed to represent the potential energy contribution to $S(\mathbf{x}(u))$ as

$$V_{\mathrm{eff}} = \frac{1}{\beta\hbar}\int_0^{\beta\hbar} \mathrm{d}u \left[V(\mathbf{x}(u)) + \frac{\sigma^2(u)}{2}\sum_{j=1}^{3N} V_{jj}(\mathbf{x}(u))\right] \tag{6}$$

where $V_{jj}(\mathbf{x}(u))$ corresponds to the second derivative with respect to coordinate j and

$$\sigma^2(u) = \frac{u}{\beta m}(\beta\hbar - u) - \sum_{k=1}^{k_{\max}} \sigma_{\mathrm{k}}^2 \sin^2\left(\frac{k\pi u}{\beta\hbar}\right) \tag{7}$$

The partition function can then be written as

$$Q = J\int \mathrm{d}\mathbf{x}\, \mathrm{d}\mathbf{a} \exp\left\{-\sum_k \mathbf{a}_k^2/2\sigma_k^2 - \beta V_{\mathrm{eff}}\right\} \tag{8}$$

where the differential element over all possible paths $D(\mathbf{x}(u))$ is replaced by $\mathrm{d}\mathbf{x}\ \mathrm{d}\mathbf{a}$ and J is a constant. This form of the partition function is ideal for a Metropolis Monte Carlo simulation which samples over coordinate space variables $\mathbf{x}$ and the Fourier coefficients, $\mathbf{a}$, using the weight function

$$W(\mathbf{x},\mathbf{a}) = \exp\left\{-\sum_k \mathbf{a}_k^2/2\sigma_k^2 - \beta\langle V_{\mathrm{eff}}\rangle\right\} \tag{9}$$

$\langle\cdots\rangle_{\mathrm{MC}}$ will indicate averages obtained by sampling with this weight function.

The thermal average of the potential energy can be estimated as $\langle\cdots\rangle_{\mathrm{MC}}$. The potential energies of the sampled configurations can be binned to generate potential energy distributions at a specified temperature. The thermal average of the total energy, $\langle E\rangle$, the kinetic energy, $\langle K\rangle$, and the specific heat, C_v, are given by

$$\langle E\rangle = \frac{3N(k_{\max}+1)}{2\beta} - \left\langle \sum_k \frac{a_k^2}{2\beta\sigma_k^2} - V_{\mathrm{eff}} - G_{\mathrm{eff}}\right\rangle_{\mathrm{MC}} \tag{10}$$

$$\langle K\rangle = \frac{3N(k_{\max}+1)}{2\beta} - \left\langle \sum_k \frac{a_k^2}{2\beta\sigma_k^2} - G_{\mathrm{eff}}\right\rangle_{\mathrm{MC}} \tag{11}$$

$$C_v/k_{\mathrm{B}} = \frac{3N(k_{\max}+1)}{2} - \left\langle \sum_k \frac{a_k^2}{\sigma_k^2} - (2G_{\mathrm{eff}}/\beta)\right\rangle_{\mathrm{MC}} + \beta^2\left\langle\left[\sum_k \frac{a_k^2}{2\beta\sigma_k^2} - V_{\mathrm{eff}} - G_{\mathrm{eff}}\right]^2\right\rangle_{\mathrm{MC}} - \beta^2\left\langle \sum_k \frac{a_k^2}{2\beta\sigma_k^2} - V_{\mathrm{eff}} - G_{\mathrm{eff}}\right\rangle_{\mathrm{MC}}^2 \tag{12}$$

where G_{eff} is a correction term related to the partial averaging procedure. The isosteric enthalpy of sorption, q_{st}, is defined as $-\Delta H_{\mathrm{st}}$, where ΔH_{st} is the enthalpy change when one mole of a gas is sorbed at a fixed concentration in the sorbent. Assuming that the helium vapor in equilibrium can be treated as a classical ideal gas, $q_{\mathrm{st}} = \langle E\rangle - {}^5/_2 RT$. In the case of a classical sorbate, this reduces to $q_{\mathrm{st}} = \langle V\rangle - RT$.

In addition to providing the equilibrium distribution of spatial coordinates, the FPIMC technique samples paths characterized by the spatial coordinates $\mathbf{x}$ at $u = 0$ and the associated Fourier coefficients $\mathbf{a}$. To analyze the nature of the sampled quantum paths, a few simple parameters were defined for the paths associated with a tagged particle i. Let $\boldsymbol{r}_i = \{x_i,y_i,z_i\}$ be the position of the the tagged particle at $u = 0$. Let $\boldsymbol{a}^x = \{a_k^x\}$, $\boldsymbol{a}^y = \{a_k^y\}$, and $\boldsymbol{a}^z = \{a_k^z\}$ be the associated sets of Fourier coefficients. The canonical ensemble average of the net displacement along a quantum path, in general, is very nearly zero. However, the canonical ensemble average of the mean square displacement along a quantum path is nonzero and is defined as

$$\langle d^2\rangle = \left\langle \int_0^{\beta\hbar} |\mathbf{r}(u) - \mathbf{r}(0)|^2\, \mathrm{d}u\right\rangle = 1.5\sum_{k=1}^{k_{\max}} \langle (a_k^x)^2\rangle \tag{13}$$

In the case of a free particle, $\langle d^2\rangle = (3\beta\hbar^2/m\pi^2)\sum_1^{\infty}(1/k^2) = \sqrt{\beta\hbar^2/2m}$. For a particle in a confining potential, an upper bound to λ^2 can be defined as

$$\lambda^2 = \langle d^2\rangle + \frac{3\beta\hbar^2}{m\pi^2}\left\{\frac{\pi^2}{6} - \sum_1^{k_{\max}} \frac{1}{k^2}\right\} \tag{14}$$

by assuming that Fourier coefficients with $k \geq k_{\max}$ are Gaussian distributed and essentially decoupled from the potential. Thus the effect of the confining potential on the extent of quantum

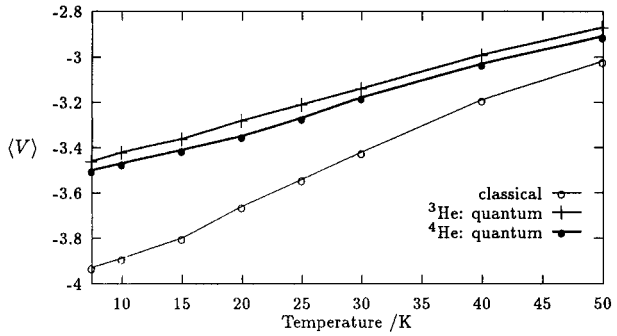

Figure 2. Average potential energy (in kJ mol^{-1}) as a function of temperature for helium in silicalite in the dilute limit. Error bars for $\langle V \rangle$ and $\langle V_{\text{eff}} \rangle$ are less than 2% for all the simulations.

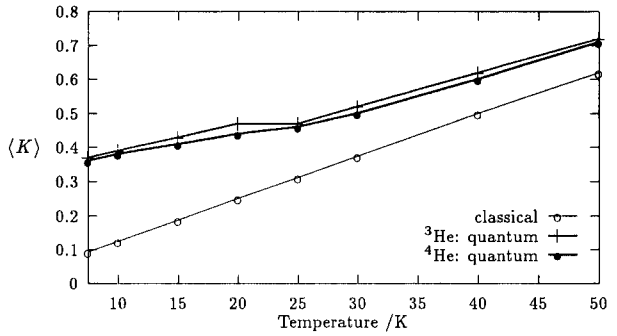

Figure 3. Average kinetic energy (in kJ mol^{-1}) as a function of temperature for helium in silicalite in the dilute limit. Error bars for $\langle K \rangle$ are approximately 10% at the lowest temperatures and are on the order of 5% or less for temperatures above 15 K.

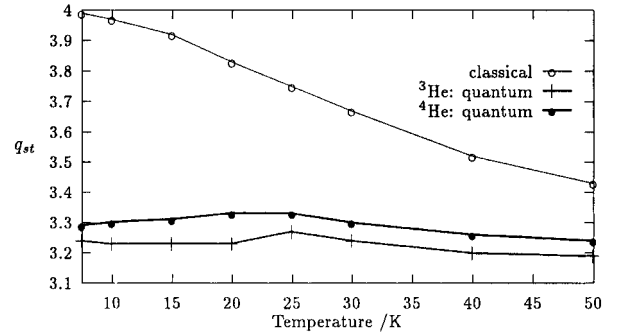

Figure 4. Isosteric heats of adsorption, q_{st} (in kJ mol^{-1}), for helium in silicalite in the dilute limit. Error bars for q_{st} are less than 3% for all the simulations.

delocalization can be judged by the ratio $\lambda/\lambda_{\text{free}}$. If λ is much smaller than the average interparticle separation, superfluidity is unlikely.

4. Computational Details

FPIMC and classical MC simulations were carried out using periodic boundary conditions with the simulation cell consisting of two unit cells of silicalite aligned along the *z*-axis. The sorbate zeolite interaction energy was found to be converged to better than 1% for this size of simulation cell. Unless otherwise stated, all simulations reported here are for a single sorbate particle in the simulation cell. The temperature range of the simulations was from 7.5 to 50 K.

The principal computational cost is due to the evaluation of the pair potential with the zeolite lattice atoms. In the case of a rigid lattice, this cost can be decreased by at least an order of magnitude by pretabulating the potential over a mesh of equispaced points covering the asymmetric unit. A scheme combining quadratic interpolation in the *z*-direction with bicubic interpolation in the *x*,*y*-plane was used to interpolate between points on the mesh.[39] A mesh spacing of 0.18 Å in each direction provided accuracy to at least the fourth significant figure in the potential energy. To prevent any instability in the MC simulations due to inaccuracies in the interpolation scheme for very high or very low potential energy regions, a direct evaluation of the interaction potential was carried out whenever the interpolated value was outside the range − 12 to 12 kJ/mol.

In a single trial move for the FPIMC simulations, the first four to six Fourier coefficients were changed with probabilities proportional to 1/*k*, and all the remaining coefficents and the spatial coordinates were moved simultaneously. The integration over imaginary time *u* to obtain V_{eff} was carried out by trapezoidal quadrature with N_{quad} points. For temperatures above 20 K, $k_{\text{max}} = 1$ and $N_{\text{quad}} = 4$ was sufficient for converging the total energy, $\langle E \rangle$, to within the statistical error. For temperatures between 20 and 6 K, $k_{\text{max}} = 4$ and $N_{\text{quad}} = 4$ were found to be adequate, while at 2 K, $k_{\text{max}} = 8$ and $N_{\text{quad}} = 8$ were used. Monte Carlo run lengths of 2.5−5 million were used.

5. Results

The simplest indicator of the importance of quantum effects is provided by a comparison of the values of various thermodynamic averages obtained from the FPIMC and classical MC simulations. Figures 2 and 3 show the dependence of $\langle V_{\text{eff}} \rangle$ and $\langle K \rangle$, respectively, on temperature. For ^{3}He, the maximum increase in the average potential energy with respect to the classical value is 12%, and the increase in the kinetic energy due to quantum delocalization effects is 300%. Isotope effects on $\langle V_{\text{eff}} \rangle$ and $\langle K \rangle$ are on the order of 5%−10%. Figure 4 shows q_{st} as a function of temperature. A major qualitative difference between the q_{st} curves obtained from the quantum and classical simulations is that q_{st} for the quantum system is virtually constant at ∼3.3 kJ mol^{-1} temperature, while for the classical system it increases significantly with decrease in temperature. The difference between the quantum and classical values of q_{st} ranges from 23% at 7.5 K to 4% at 50 K for ^{4}He in silicalite. At present, no published experimental data is available for q_{st} for He adsorbed in silicalite. However, q_{st} values for silica-Y are available and are approximately 1.6 kJ/mol in the temperature range of the simulations. While q_{st} will be affected by the zeolite structure, it will depend primarily on the strength of binding to the silicate wall for dilute concentrations. Therefore q_{st} would be expected to be very similar for different high-silica zeolites. Thus it would appear that the present potential predicts far too high guest−host binding energies. In this context it is interesting to note that neutron diffraction experiments suggest an even lower binding energy of 0.33 kJ/mol. C_v/k_{B} values obtained from the simulations are plotted in Figure 5. The C_v/k_{B} curve goes through a maximum and then starts to decrease. For the quantum system, the specific heat again starts to increase at about 8 K, but given the large statistical errors in the specific heat at low temperature, further simulations are necessary to establish whether this is a physically significant effect. The quantum values are consistently lower than the classical values by a factor of 1.5−2 except at the lowest temperatures. In view of the statistical uncertainity in the specific heat and the necessity for improving the potential energy surface, quantitative comparison of specific heats obtained experimentally and theoretically would appear to be premature.

The distribution of potential energies sampled during the course of a simulation provides an indication of the types and energies of adsorption sites provided by the sorbent. Figure 6a shows that at 10 K the classical distribution is much narrower

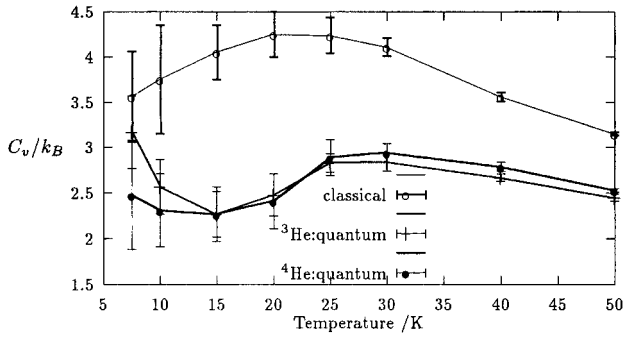

Figure 5. Specific heat, C_v/k_B, as a function of temperature. Error bars for each simulation are shown.

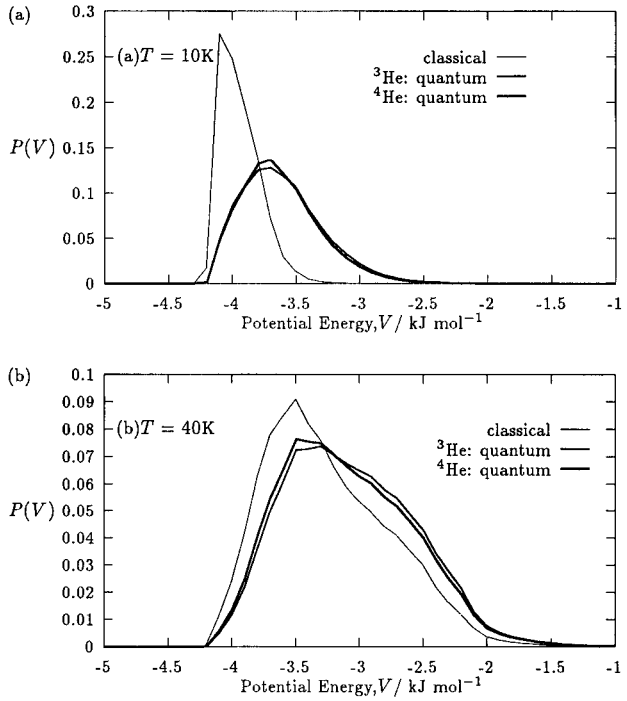

Figure 6. Potential energy distributions, $P(V)$, derived from classical and quantum simulations of helium in silicalite at (a) 10 K and (b) 40 K.

TABLE 2: FPIMC Simulation Averages for ^{4}He in Silicalite at 10 K as a Function of the Strength of the Helium−Silicalite Interaction

	$\langle V\rangle$ (kJ/mol)	$\langle V_{\text{eff}}\rangle$ (kJ/mol)	$\langle K\rangle$ (kJ/mol)	$\langle E\rangle$ (kJ/mol)	C_v/k_B	$\lambda/\lambda_{\text{free}}$	λ (bohr)
$1.25\epsilon_{\text{HeO}}$	−4.59	−4.45	0.44	−4.01	2.1	0.53	0.78
ϵ_{HeO}	−3.57	−3.47	0.38	−3.09	2.3	0.55	0.81
$0.75\epsilon_{\text{HeO}}$	−2.60	−2.53	0.32	−2.21	2.2	0.57	0.84

and peaks at a lower energy than the corresponding quantum disribution, but by 40 K, the quantum and classical distributions are virtually identical, as shown in Figure 6b.

To test the effect of the confining potential on the degree of quantum delocalization, Table 2 shows simulation averages for three different values of the ϵ_{OHe} parameter. Changes in λ are relatively small when ϵ is varied even though the q_{st} values are altered substantially; however, a stronger lattice−sorbate interaction does lower the value of λ. In general, it would appear that the strong binding to the zeolite wall reduces the extent of quantum fluctuations.

6. Conclusions

The present study constitutes the first application of path integral Monte Carlo methods to helium adsorption in zeolites and leads to several important qualitative conclusions. Quantum effects are shown to modify isosteric heats of adsorption, q_{st}, by up to 25% and specific heats, C_v, by up to 60% in the temperature range 10−20 K. Isotope effects are small in the temperature range studied from 7.5 to 50 K, in comparison to the absolute magnitudes of the binding energy. The root mean square quantum path length fluctuation is a useful measure of the effect of the confining potential on the degree of quantum delocalization. The strong potential exerted by the silicalite lattice is shown to appreciably reduce quantum fluctuations in the path lengths of helium atoms.

The path integral Monte Carlo formulation presented here can be extended to higher concentrations and lower temperatures. The extent of quantum effects demonstrated for the helium−silicalite system indicates that finite temperature quantum simulations will be essential for obtaining improved helium−zeolite potential energy surfaces by fitting to experimental data on isosteric heats of sorption.

Acknowledgment. I am grateful to the Computer Science and Engineering department of I.I.T-Delhi for providing computational resources. I would like to thank S. D. Mahanti for getting me interested in the problem of helium adsorption in confined media. It is a pleasure to acknowledge useful discussions with S. Yashonath, A. Ramanan, A. K. Ganguli, and R. Ramaswamy.

References and Notes

(1) Barrer, R. M. *Zeolites and Clay Minerals as Sorbents and Molecular Sieves*; Academic Press: New York, 1978.
(2) Breck, D. W. *Zeolite Molecular Sieves*; Wiley Interscience: New York, 1974.
(3) Yashonath, S.; Santikary, P. *Phys. Rev. B* **1992**, *45*, 10095.
(4) Titiloye, J. O.; Parker, S. C.; Stone, F. S.; Catlow, C. R. A. *J. Phys. Chem.* **1991**, *95*, 4038.
(5) June, R. L.; Bell, A. T.; Theodorou, D. N. *J. Phys. Chem.* **1990**, *94*, 8232.
(6) Smit, B.; Siepmann, J. I. *Science* **1994**, *264*, 1118.
(7) Amrani, S. E.; Vigne-Maeder, F.; Bigot, B. *J. Phys. Chem.* **1992**, *96*, 9417.
(8) Bifone, A.; Pietrass, T.; Kritzenberger, J.; Pines, A.; Chmelka, B. F. *Phys. Rev. Lett.* **1995**, *74*, 3277.
(9) Vigne-Maeder, F. *J. Phys. Chem.* **1994**, *98*, 4666.
(10) Li, F.-Y.; Berry, R. S. *J. Phys. Chem.* **1995**, *99*, 2459.
(11) Saunders, M.; Jimenez-Vazquez, H. A.; Cross, R. J.; Billups, W. E.; Gesenberg, C.; Gonzalez, A.; Luo, W.; Haddon, R. C.; Diederich, F.; Hermann, A. *J. Am. Chem. Soc.* **1995**, *117*, 9305.
(12) Sokol, P. E.; Gibbs, M. R.; Stirling, W. G.; Azuah, R. T.; Adams, M. A. *Nature* **1996**, *379*, 616.
(13) Moon, K.; Girvin, S. M. *Phys. Rev. Lett.* **1995**, *75*, 1328.
(14) Cheng, E.; Cole, M. W.; Dupont-Roc, J.; Saam, W. F.; Treiner, J. *Rev. Mod. Phys.* **1993**, *65*, 557.
(15) Stringari, S.; Treiner, J. *J. Chem. Phys.* **1987**, *87*, 5021.
(16) Pricaupenko, L.; Treiner, J. *Phys. Rev. Lett.* **1995**, *74*, 430; **1994**, *72*, 2215.
(17) Abraham, F. F.; Broughton, J. Q. *Phys. Rev. Lett.* **1987**, *59*, 64.
(18) Konishi, K.; Deguchi, H.; Takeda, K. *J. Phys.: Condens. Matter* **1993**, *5*, 1619.
(19) Wada, N.; Kato, H.; Watanabe, T. *J. Low Temp. Phys.* **1994**, *95*, 507.
(20) Kato, H.; Ishioh, K.; Wada, N.; Ito, T.; Watanabe, T. *J. Low Temp. Phys.* **1987**, *68*, 321.
(21) Wada, N.; Ishioh, K.; Watanabe, T. *J. Phys. Soc. Jpn.* **1992**, *61*, 931.
(22) Wada, N.; Kato, H. *Physica B* **1994**, *194*, 685.
(23) Fang, M. P.; Sokol, P. E. *Phys. Rev. B* **1995**, *52*, 12614. Fang, M. P.; Sokol, P. E.; Wang, Y. *Phys. Rev. B* **1994**, *50*, 12291.
(24) Schmidt, K. E.; Ceperley, D. M. In *The Monte Carlo Method in Condensed Matter Physics*; Binder, K., Ed.; Springer-Verlag: Berlin, 1992.
(25) Ceperley, D. M. *Rev. Mod. Phys.* **1995**, *67*, 279.
(26) Chen, B. Y.; Mahanti, S. D.; Yussouff, M. *Phys. Rev. Lett.* **1995**, *75*, 473.
(27) Chen, B. Y.; Mahanti, S. D.; Yussouff, M. *Phys. Rev. B* **1995**, *51*, 5800.
(28) Bezus, A. G.; Kiselev, A. V.; Lopatkin, A. A.; Du, P. Q. *J. Chem. Soc., Faraday Trans. 2* **1978**, *74*, 367.

(29) Kiselev, A. V.; Du, P. Q. *J. Chem. Soc., Faraday Trans. 2* **1981**, *77*, 1.
(30) Kiselev, A. V.; Lopatkin, A. A.; Shulga, A. A. *Zeolites* **1985**, *5*, 261.
(31) Pellenq, R. J.-M.; Nicholson, D. *J. Phys. Chem.* **1994**, *98*, 13339.
(32) Maitland, G. C.; Rigby, M.; Smith, E. B.; Wakeham, W. A. *Intermolecular Forces: Their Origin and Determination*; Clarendon: Oxford, 1981.
(33) Miller, T. M.; Bederson, B. *Adv. At. Mol. Phys.* **1977**, *13*, 1.
(34) Meier, W. M.; Olson, D. H. *Atlas of Zeolite Structure Types*; Butterworth: London, 1988.
(35) Freeman, D. L.; Doll, J. D. *Adv. Chem. Phys.* **1988**, *70*, 139.
(36) Doll, J. D.; Freeman, D. L.; Beck, T. L. *Adv. Chem. Phys.* **1990**, *78*, 61.
(37) Frantz, D. D.; Freeman, D. L.; Doll, J. D. *J. Chem. Phys.* **1992**, *97*, 5713.
(38) Chakravarty, C. *J. Chem. Phys.* **1995**, *102*, 956. Chakravarty, C. *Mol. Phys.* **1995**, *84*, 845. Chakravarty, C. *Phys. Rev. Lett.* **1995**, *75*, 1727. Chakravarty, C. *J. Chem. Phys.* **1995**, *103*, 10663. Chakravarty, C. *J. Chem. Phys.* **1996**, *104*, 7223.
(39) Press, W. H.; Flannery, B. P.; Teukolsky, S. A.; Vetterling, W. T. *Numerical Recipes: The Art of Scientific Computing*; Cambridge University Press: Cambridge, 1989.